



Full paper

## Zigzag or spiral-shaped nanostructures improve mechanical stability in yttria-stabilized zirconia membranes for micro-energy conversion devices



Yanuo Shi<sup>a</sup>, Aline Fluri<sup>b,c</sup>, Inigo Garbayo<sup>a,d</sup>, J. Jakob Schwiedrzik<sup>e</sup>, Johann Michler<sup>e</sup>, Daniele Pergolesi<sup>b,f</sup>, Thomas Lippert<sup>b,g</sup>, Jennifer Lilia Marguerite Rupp<sup>a,h,i,\*</sup>

<sup>a</sup> Electrochemical Materials, Department of Materials, ETH Zürich, Switzerland

<sup>b</sup> Laboratory for Multiscale Materials Experiments, Paul Scherrer Institute, 5232, Villigen PSI, Switzerland

<sup>c</sup> Faculty of Engineering, Kyushu University, Fukuoka, Japan

<sup>d</sup> Area of Advanced Materials for Energy, Catalonia Institute for Energy Research (IREC), Barcelona, Spain

<sup>e</sup> EMPA Swiss Federal Laboratories for Materials Science and Technology, Laboratory for Mechanics of Materials and Nanostructures, Thun, Switzerland

<sup>f</sup> Electrochemistry Laboratory, Paul Scherrer Institute, 5232, Villigen PSI, Switzerland

<sup>g</sup> Department of Chemistry and Applied Biosciences, Laboratory of Inorganic Chemistry, ETH Zürich, Switzerland

<sup>h</sup> Electrochemical Materials, Department of Material Science and Engineering, MIT, USA

<sup>i</sup> Electrochemical Materials, Department of Electrical Engineering and Computer Science, MIT, USA

### ARTICLE INFO

#### Keywords:

Energy conversion membrane  
Zigzag nanomorphology  
Mechanical stability  
Micro-solid oxide fuel cell

### ABSTRACT

Free-standing solid-state ion conducting thin film membranes are key components in micro-energy conversion devices such as micro-solid oxide fuel cells or electrolyzers. Through this work, we explore the design and fabrication of thin film architectures with either straight, zigzag or spiral-shaped columnar grain nanostructures of 8 mol% doped Yttria stabilized zirconia (8YSZ) in order to modify the ceramics elastic properties and mechanical stability for MEMS integration. We report that the zigzag and spiral-shaped nanomorphologies' can be engineered with a ~44% reduced elastic modulus. Ultimately, this results in an increased fabrication yield when the thin ionic conductor thin film structures are turned into free-standing membranes as required for different micro energy converter applications. Raman spectroscopy reveals that the symmetry is lowered by the existence of monoclinic distortions in the cubic phase which modifies the elastic moduli of films with straight columnar structures. Fundamentally, we show here evidence that for yttria-stabilized zirconia modifications in membrane nano-architectures and strain can lead to phase changes, which agrees well with findings published in the 1970s based on applied external stress's on macroscopic structures (i.e. pellets). The influence of the change in nanomorphology on the cross-plane ionic conductivity is minor. The oxygen ion conducting thin film nanomorphology design exhibits potential to optimize grain connectivity and tortuosity by growth as either columnar, zigzag or spiral-shaped morphologies, in order to obtain membranes with controllable phases and elastic moduli for micro-energy conversion devices.

### 1. Introduction

Enhancing the charge carrier transport and mechanical stability of solid state ionic thin films plays a significant role in optimizing the performance of next generation of micro-energy conversion and information storage devices such as, e.g. micro-solid oxide fuel cells (micro-SOFCs) [1–3], microbatteries [4–9] or memristors operating on resistive switching [10–16]. It is well-known that the ionic transport of an oxide such as ceria or zirconia can be altered by the addition of an extrinsic dopant and tuning its concentration [17–19]. Furthermore, recent research shows that manipulation of lattice strain can affect the

total conductivity by changing the ionic migration volume [20–25], the oxygen surface exchange [26], the redox-state, breaking locally lattice symmetry [14] or even suppress phase change keeping the oxides in the fast ionic conducting phase [27].

Regarding the electrolyte material, Yttria-stabilized zirconia (YSZ), eg. 8 mol%  $Y_2O_3$  doped  $ZrO_2$  (8YSZ), is a good choice for thin film-based energy conversion devices due to its purely ionic conductivity. YSZ offers very good physiochemical stability when compared to currently discussed perovskite electrolytes which shows phase stability challenges [28]. In micro-energy conversion devices such as micro-SOFCs, the YSZ electrolyte is integrated as a thin film free-standing

\* Corresponding author. Electrochemical Materials, Department of Material Science and Engineering, MIT, USA.

E-mail address: [jrupp@mit.edu](mailto:jrupp@mit.edu) (J.L.M. Rupp).

<https://doi.org/10.1016/j.nanoen.2019.03.017>

Received 15 January 2019; Received in revised form 4 March 2019; Accepted 4 March 2019

Available online 11 March 2019

2211-2855/ © 2019 Elsevier Ltd. All rights reserved.

membrane with a thickness of several hundred nanometers separating both electrodes and gas compartments [1,29–33]. Successful integration and operation of micro-SOFC membranes based on 8YSZ free-standing membranes were for example demonstrated for YSZ films fabricated by spray pyrolysis [34], pulsed laser deposition [35], Rf sputtering [36], dc sputtering [37] and atomic layer deposition [30] processing. Micro-SOFCs are typically integrated on a Si-based substrate to be MEMS compatible and can achieve high power densities (eg. up to  $1300 \text{ mW/cm}^2$  [28]). The free-standing electrolyte in micro-SOFCs is conventionally obtained by depositing the ceramic thin film on a free-standing  $\text{Si}_3\text{N}_4$  template and subsequently removing the underlying layer by microfabrication techniques (e.g. removing  $\text{Si}_3\text{N}_4$  by reactive ion etching, RIE), see Ref. [3] for detail. Here, a critical aspect is the mechanical stability of the oxygen-ion conducting membrane which depends on its specific nanomorphology in terms of the average grain size, the kind and extent of the grain boundary regions, the shape and facets of the grains and the overall stress state. All these aspects are to some extent related and may be affected by the processing choice. The aim of this study is to grow YSZ films on the amorphous surface of the sacrificial  $\text{Si}_3\text{N}_4$  layer with different nanomorphologies by selecting different deposition conditions of pulsed laser deposition (PLD). Thus, we identify morphological features, which lead to improved thermo-mechanical properties of the electrolyte free-standing membrane.

Conventionally in PLD, the incoming particle flux is kept normal to the substrate surface ( $\alpha$ , the angle between the surface normal and the direction of the so-called ablation plume, is  $0^\circ$ ). For YSZ this often results in a nanomorphology characterized by straight and columnar grains perpendicular to the substrate surface, see Fig. 1a and e.g. Heiroth et al. [38]. Nanoindentation experiments detected elastic moduli of around  $294.8 \pm 44.8 \text{ GPa}$  for polycrystalline 8YSZ films with the cubic phase. Recently, Stender et al. demonstrated that the elasticity of YSZ thin films grown on  $\text{Al}_2\text{O}_3$  can be successfully modified by employing pulsed laser deposition with  $\alpha \geq 45^\circ$  [39]. A non-perpendicular angle of incidence produces a shadowing effect, meaning that one side of the nucleated, island-like grain is shaded from the particle flux, so that the grain grows faster on the side facing the ablation plume. Consequently, a columnar growth no longer yields perpendicular but tilted grain columns. By rotating the substrate at certain intervals, so does the direction of the grain growth for the oxide film. As shown in Fig. 1a. If  $\alpha = 0^\circ$ , a film with typical, columnar morphology is obtained consisting of parallel adjacent pillars oriented perpendicularly to the substrate surface. If  $\alpha = 60^\circ$ , the columns are inclined by  $\sim 35^\circ$  with respect to the substrate surface normal. Rotating the sample by  $180^\circ$  halfway through the deposition results in a zigzag-shaped thin film nanomorphology;  $90^\circ$  rotation after each quarter of the deposition gives a rectangular spiral (henceforth called spiral-shaped). It is noted that the spiral structure is different from the zigzag samples fabricated by Stender et al. [39]). In the so-called oblique angle deposition, tilted grains appear typically only above a certain threshold angle whereby  $\alpha \leq 70^\circ$  typically yields highly dense films, while  $\alpha \geq 80^\circ$  is used to produce porous nanomorphologies [40,41]. A dense structure may be promoted by high deposition temperatures or a high kinetic energy of the incoming species [41]. With this technique, the typically straight columnar morphology of YSZ thin films on  $\text{Al}_2\text{O}_3$  substrates was modified to zigzag shaped columns (grains inclined by  $36^\circ$  for  $\alpha \geq 45^\circ$ ). Such films were shown to be  $\sim 35\%$  more elastic (resulting in an elastic modulus of around  $250 \text{ GPa}$ ) as compared to films with the typical straight columns perpendicular to the substrate [39]. That various zigzag-related nanomorphologies are more elastic than their straight columnar counterparts has also been demonstrated for other materials including porous chromium or titania deposited by sputtering or PLD under oblique angles [42,43]. The zigzag- or spiral-shaped winding (“tortuosity”) of the grains can be visualized as forming “micro-springs”, making the material more elastic [44].

In this study, in addition to exploring the possibilities of different oblique angle deposition options, we study the relationships between

ionic transport, elastic properties and phase stability of ion-conducting 8YSZ free-standing thin film membranes with tailored nanomorphologies, for application in real devices. Mechanically induced phase changes in Yttria-stabilized zirconia and potential symmetry lowering by externally applied stress have been reported already 30 years ago for bulk processed pellets [45,46]. This effect is also known for polycrystalline thin film structures, where phase symmetry lowering can be induced by the interfacial strain between film and substrate [34]. In other words, a part of the stress can be accommodated through lattice distortions, which in turn lower the symmetry of the crystal structure. However, the phase stability of 8YSZ when processed as free-standing thin film membranes under mechanical strain is still unclear and requires attention. From a fundamental perspective, the understanding of electro-chemo-mechanics for oxygen ionic conductors based on zirconia or ceria is important to establish fast ionic transfer and mechanical stability at bulk and interfaces for application in micro-energy converters. While zigzag-like nanomorphologies promise to largely modify the elastic properties of substrate-supported oxygen ion conductive films, it remains unclear how the change in nanomorphology affects: *i.* the integration as free-standing membranes for micro-energy conversion devices, *ii.* the oxygen-cation bond strength, *iii.* the crystallographic phase of zirconia (e.g. cubic, tetragonal, monoclinic), and *iv.* the oxygen ion transport across a free-standing membrane. To investigate these points we fabricated and studied thin film membranes of 8YSZ with three types of nanomorphologies, changing the grain columns' shape from straight to zigzag and spiral-like through variation of the angle  $\alpha$  between the substrate surface normal and the ablation plume. The elastic properties were studied by nanoindentation and Raman spectroscopy was employed to analyze the lattice vibrations and crystallographic phases. Finally, the cross-plane ionic conduction properties of the membranes were characterized to study the influence of the varied morphologies on the ionic transport. The possibility to tune the elastic properties of ion conducting free-standing membrane has a high potential of becoming an important building block for the design and fabrication of micro-energy converters.

## 2. Results and discussion

The YSZ thin films fabricated for the present study are schematically depicted in Fig. 1. Fig. 1a shows the working principle of oblique angle pulsed laser deposition (PLD) for the thin film growth in this study, the schematic cross-sectional view of thin films and the SEM micrographs of the straight, zigzag and spiral-shaped nanomorphologies for the 8YSZ films grown on  $\text{Si}_3\text{N}_4$  coated Si substrates. Different from the straight and zigzag structure, the tilted grown direction in every second section of deposition for the spiral-shaped nanomorphologies are in planes perpendicular to the plane seen in the SEM image. Therefore, part of the cross-section view of spiral-shaped looks vertically straight. During the deposition, the surface of the target material 8YSZ is ablated by a pulsed UV laser then the ablated species adiabatically expands towards the substrate before condensing as a thin film. For all three types of nanomorphologies, the width of the columns visible in the SEM images is around 10–20 nm in average. These 8YSZ films are used for the microfabrication of free-standing membranes. We confirm that independently on the inclination of the grains free-standing membranes of around 240 nm in thickness can be made, Fig. 1b. The optical microscopy view of the free-standing membranes is displayed for the three model nanomorphologies - ranging from straight to zigzag to spiral-shaped 8YSZ - with Pt microelectrode on top. Interestingly, we observe that the buckling pattern of the membranes changes for the three representative samples. Different buckling behavior can be explained based on the symmetry of the straight morphology being isotropic in-plane while it is 2- and almost 4-fold for the zigzag and the spiral-shaped morphology, respectively. The different symmetry of the nanomorphology likely correlates with the in-plane symmetry of the mechanical properties, thus with the buckling which is in agreement

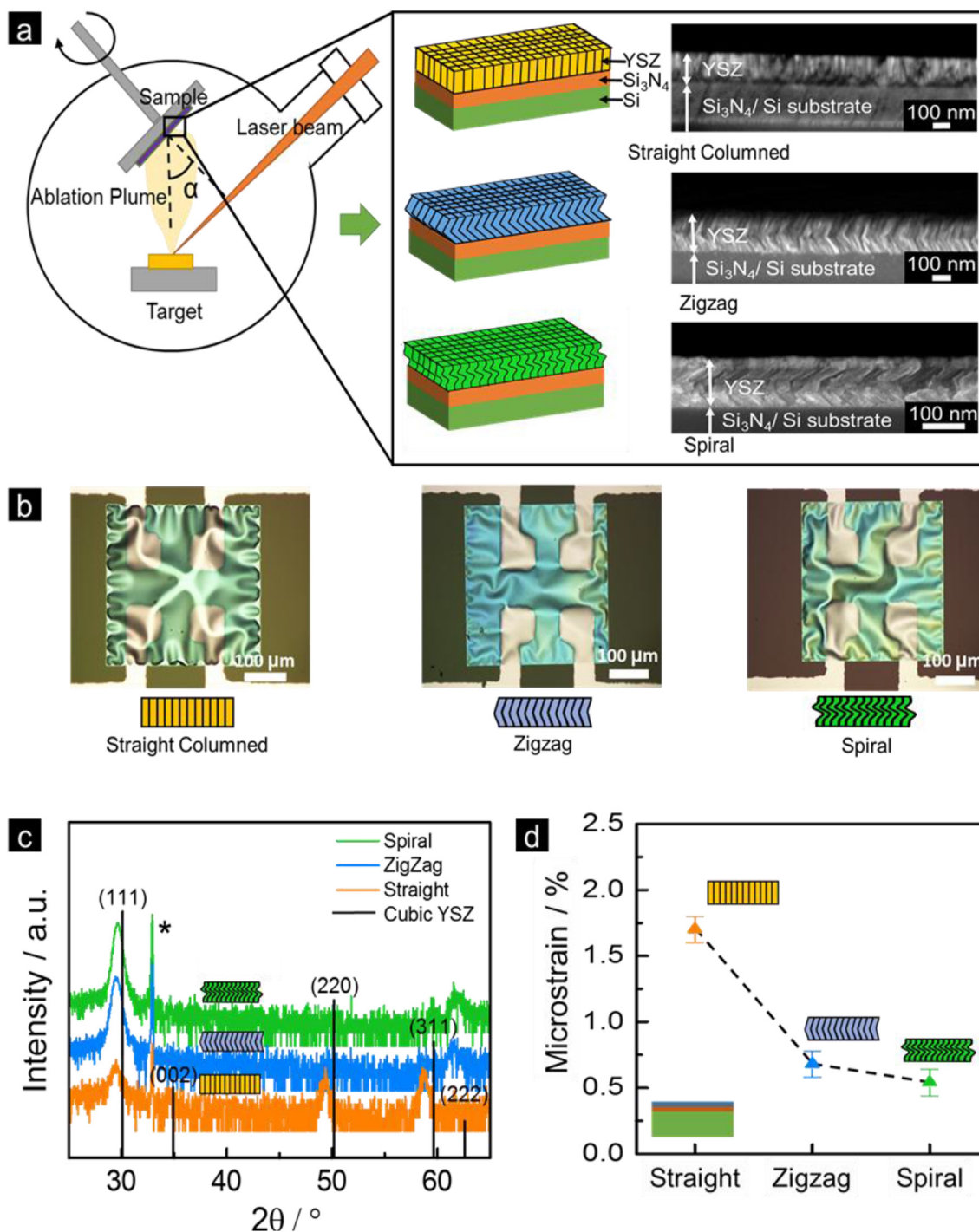


**Fig. 1.** (a) Oblique angle pulsed laser deposition for the fabrication of yttria-stabilized zirconia thin films with varied nanomorphologies and grain-grain connections to form straight columnar, zigzag and spiral-shaped structures. (b) Optical microscopy images of the free-standing membranes with straight, zigzag and spiral-shaped 8YSZ structure. Pt electrodes are on top of the membrane for following electrical characterization. (c) XRD diffractograms of straight, zigzag and spiral-shaped 8YSZ films on Si/Si<sub>3</sub>N<sub>4</sub> substrates. The reference of cubic YSZ thin film from Ref. [63] is also added for comparison. Si substrate diffraction peak is indicated with asterisk. (d) Relation between out-of-plane strain obtained from XRD result and the morphology of the substrate-supported YSZ thin films.

with Ref. [47]. X-Ray diffraction (XRD) was used to analyze the crystal structure of the thin films with different nanomorphologies. Since the non-clamped area of the free-standing membranes is much smaller than the spot size of the X-ray beam of typical thin film diffractometers (as used here) this analysis was carried out on substrate-supported YSZ films (i.e. on the Si<sub>3</sub>N<sub>4</sub> coated Si wafer) for subsequent analysis, see Fig. 1c. Analyzing the diffraction patterns of the straight, zigzag and spiral-shaped 8YSZ nanomorphologies on substrate, the (111), (200),

(220), (311) and (222) diffraction peaks of the cubic phase are observed [48,49]. The positions of the (111), (220) and (311) reflections are shifted to higher 2 theta values when the nanomorphology of the thin film is changed from the straight columnar to the zigzag and to the spiral-shaped (See Supplementary Information S1). Through the Scherrer and Willson equation [50] the out-of-plane strain values in the substrate supported 8YSZ films (obtained from XRD result) are determined as  $1.7 \pm 0.1\%$ ,  $0.68 \pm 0.1\%$  and  $0.54 \pm 0.1\%$  for the

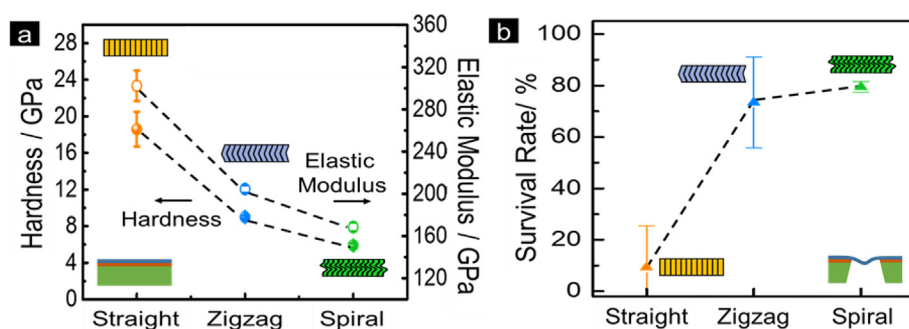


Fig. 2. Mechanical properties of 8YSZ thin films with different nanomorphologies: (a) Hardness and elastic modulus for straight, zigzag and spiral-shaped nanomorphologies of 8YSZ films on  $\text{Al}_2\text{O}_3$  substrate measured by nanoindentation. (b) Microfabrication survival rate of the free-standing 8YSZ membranes based on straight, zigzag, and spiral-shaped nanomorphologies. The average survival rates of two batches are presented and the corresponding error bars are shown.

straight, zigzag and spiral-shaped nanomorphologies, respectively, Fig. 1d.

To determine the influence of the nanomorphology on the elastic modulus, nanoindentation using a Berkovich tip is performed on YSZ films deposited on  $\text{Al}_2\text{O}_3$  substrates. It can be seen in Fig. 2a that the hardness of the thin film is decreased from  $18.6 \pm 1.9$  GPa to  $9.0 \pm 0.2$  GPa when the nanomorphology is changed from straight to zigzag shaped columns of 8YSZ film. A further decrease of the hardness to  $5.9 \pm 0.2$  GPa is measurable when the nanomorphology is changed to the spiral-shaped configuration. Note that the substrate used here differs so the absolute values might vary with respect to the free-standing YSZ films. Due to this reason we rather focus in subsequent analysis on the relative changes observed between the three nanomorphologies. The plain strain modulus  $E$  is changed by almost 50% from  $302.3 \pm 14.4$  GPa to  $204.5 \pm 3.7$  GPa and  $168.5 \pm 4.3$  GPa for a change in nanomorphology from straight to zigzag and to spiral, respectively. The results for the straight and the zigzag morphology are in good agreement with a previous study [39]. The fact that the hardness, a measure for the resistance of the material against permanent deformation, was reduced is probably due to the fact that in the zigzag and spiral-shaped nanomorphologies columnar grain boundaries were more favorably oriented with respect to the direction of maximum shear stress. This enables the sliding along columnar grain boundaries to contribute to the overall deformation more strongly as compared to the straight columnar nanomorphology. The changed elastic modulus is in line with the known anisotropy of YSZ and with the fact that in the zigzag and spiral-shaped nanomorphologies the (001) direction, which is the stiffest direction in 8YSZ [51], is more inclined with respect to the loading direction. This can be rationalized as follows: By taking the known cubic elastic constants for 8YSZ from the literature [51] and averaging the stiffness tensor in the membrane plane (Voigt average) to account for random grain orientation perpendicular to the growth direction, an out-of-plane modulus of 360 GPa and a biaxial membrane modulus  $\frac{E_{ip}}{1-\nu_{ip}} = 443$  GPa is computed for the columnar grain configuration (in plane modulus  $E_{ip} = 283$  GPa, in plane Poisson ratio  $\nu_{ip} = 0.36$ ). In order to mimic the spiral-shaped nanomorphologies, the stiffness tensor is rotated by  $35^\circ$  around the (010) axis and the elastic moduli are again averaged in the membrane plane, which yields an out-of-plane modulus of 220 GPa and a biaxial membrane modulus of 319 GPa ( $E_{ip} = 234$  GPa,  $\nu_{ip} = 0.27$ ). This is well in line with the reduction of the planar strain modulus found by nanoindentation when changing from columnar to zigzag or spiral-shaped nanomorphologies [39] and with the idea that increased stability of free-standing membranes is related to an increased membrane compliance. The zigzag and spiral-type nanomorphologies most probably also increase the fracture toughness of the membranes, which could explain the increased viability. If the grain boundaries are taken as weak interfaces, then any crack starting from a surface flaw in the columnar structures will go straight through the membrane leading to failure. For the other two morphologies, the crack would have to change direction several times, which is a toughening mechanisms, as it increases the energy the crack needs to propagate significantly.

The implication of the reduction of the elastic modulus of YSZ films (on  $\text{Al}_2\text{O}_3$ ) from  $\sim 302$  GPa to  $\sim 169$  GPa, on the survival rate of free-standing membranes during reactive ion etching (RIE) is tested for the straight, zigzag and spiral-shaped nanomorphologies. The survival rate during RIE can be considered as an indication of the mechanical stability. In Fig. 2b it is evident that the zigzag and spiral-shaped nanomorphologies resulted in a significantly higher survival rate of around 80% in contrast to about 9% survival of the straight morphology. We conclude that the change in the elastic modulus (Fig. 2a) and possibly the change in strain exemplified by the substrate-supported films (Fig. 1d) is beneficial for the mechanical stability during the processing of the structures to free-standing 8YSZ membranes (Fig. 2b). Further, we obtained similar results with a batch, where a different substrate-target distance was used exemplified in Supplementary Information S2.

Raman spectroscopy allows the distinction between, for example, the cubic and the tetragonal phase of YSZ and the spatial resolution of the Raman confocal scan spot of around one micron allows to selectively characterize a free-standing membrane. We study the near order oxygen anionic-cationic vibrational changes in the free-standing YSZ thin films for the three types of nanomorphology (straight, zigzag, and spiral-shaped columns), Fig. 3. A square area with a side length of around  $20 \mu\text{m}$  in the center of the membranes is selected for the Raman measurements. The obtained Raman spectra are analyzed by a Gaussian fit which allowed us to assign the peaks to different symmetric and asymmetric O–Zr–O Raman active vibrational modes. In Fig. 3a, the spectra of the three types of samples are presented. Independently of the different nanomorphology of each sample, all of them revealed mixed phases, matching previously reported results on 8YSZ thin films [48,52,53]. The high-intensity peak at  $\sim 610 \text{ cm}^{-1}$  is assigned to the  $F_{2g}$  symmetric stretching vibrational mode of Zr–O bonds of the cubic YSZ phase. Besides that, other small peaks are also observed in the spectrum, which can be ascribed to a monoclinic phase distortion reported for solid solutions of zirconia and Ytria. For example, the Raman signatures at  $\sim 148 \text{ cm}^{-1}$  and  $\sim 490 \text{ cm}^{-1}$  are representative of  $B_g$  vibrational Raman modes; peaks at  $\sim 202 \text{ cm}^{-1}$ ,  $\sim 305 \text{ cm}^{-1}$  correspond to the  $A_g$  modes; peak at  $\sim 357 \text{ cm}^{-1}$ , assigned to  $B_u$  vibrational modes [53]. Importantly, we want to raise the attention that, after comparing the Raman measurements of the three morphologies, the small monoclinic peaks are more obvious and distinguishable in the spectra of straight 8YSZ columns, highlighting a lower symmetry and higher phase mixture degree in that type of membranes. This also coincides with the lowest mechanical stability of thin film membranes with this type of nanomorphology.

Fig. 3b is the comparison of the peak position of main the Raman vibrational modes of the three nanomorphologies of straight, zigzag, spiral-shaped columns as free-standing membranes for 8YSZ. The analysis of the peak position shift reveals the following characteristics. First, the  $A_g$  mode at  $\sim 200 \text{ cm}^{-1}$ ,  $300 \text{ cm}^{-1}$ ,  $B_u$  mode at  $\sim 350 \text{ cm}^{-1}$ , and  $B_g$  mode at  $\sim 490 \text{ cm}^{-1}$ , assigned to the monoclinic phase, exhibit scatter greater than 3 wavenumbers due to spectral noise. These peaks are weaker compared with the other modes, what makes their signal-to-noise ratio very low, influencing the total error bar. Hence, to derive a

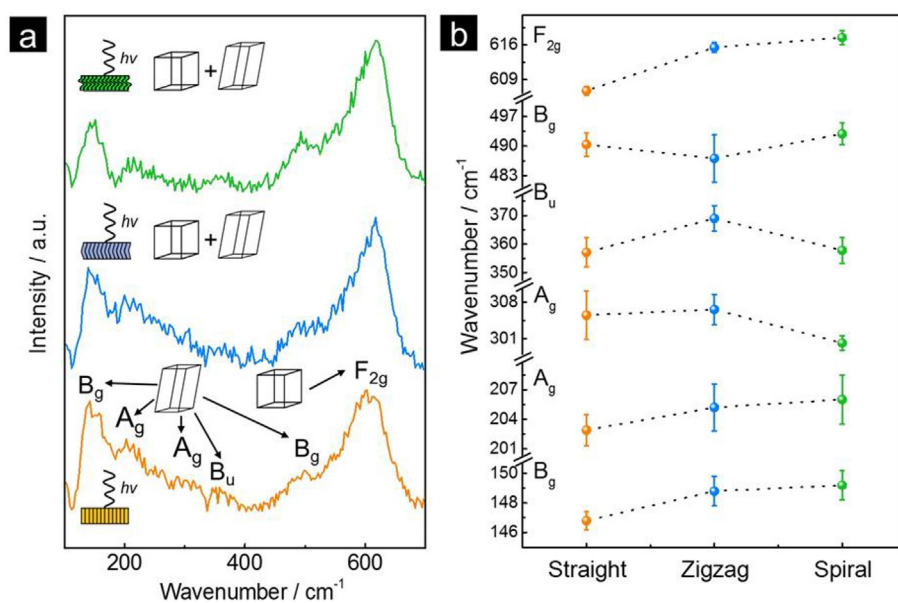


**Fig. 3.** Atomistic near order characteristics of free-standing 8YSZ thin films with different nanomorphologies through micro-Raman spectroscopy. (a) Raman spectra of free-standing 8YSZ films with straight, zigzag and spiral-shaped columned structure. The lattice structure reflected by Raman is also shown as inset. The peak of  $F_{2g}$  mode of cubic phase is observed as well as the  $A_g$ ,  $A_u$  and  $B_g$  mode which were assigned to monoclinic distortions i.e. a symmetry lowering. (b) Comparison of center positions of each mode from figure a receptivity, in order to obtain near order information of the local strain or lattice structure condition of three kinds of thin films.

reliable conclusion within the experimental error we focus our analysis on the  $B_g$  ( $\sim 148 \text{ cm}^{-1}$ ) and  $F_{2g}$  ( $\sim 610 \text{ cm}^{-1}$ ) modes. We observe that the  $B_g$  monoclinic mode around  $148 \text{ cm}^{-1}$  is shifted to a larger wavenumber when the nanomorphology is modified from straight to zigzag and to spiral-shaped columns, i.e. from  $146.8 \pm 0.6 \text{ cm}^{-1}$  (straight) to  $148.8 \pm 1.0 \text{ cm}^{-1}$  (zigzag) and then  $149.2 \pm 1.0 \text{ cm}^{-1}$  (spiral), see further details in Supplementary Information S3. Consistently, it is observed that the  $F_{2g}$  cubic mode is increased from  $606.7 \pm 0.9 \text{ cm}^{-1}$  for the straight to  $615.5 \pm 1.0 \text{ cm}^{-1}$  for zigzag and  $617.5 \pm 1.4 \text{ cm}^{-1}$  for the spiral-shaped nanomorphology. This implies an enhancement of Raman mode by  $+\Delta 2.4 \text{ cm}^{-1}$  for this  $B_g$  mode and of  $+\Delta 10.8 \text{ cm}^{-1}$  for the  $F_{2g}$  mode, with a reduction of the elastic modulus from  $\sim 302 \text{ GPa}$  to  $\sim 169 \text{ GPa}$  when changing the nanomorphology. It is important to note that in this study negligible changes in the peak position are expected from the small change in grain size between samples [54], or from possible heating effects due to applied laser power [55]. Also, all the measurements were taken in free-standing thin films, so the observed changes can only be ascribed to changes in morphology, and not to the fact of being released from the substrate. Meanwhile, it is reported that a shift of a Raman mode to larger wavenumbers may reflect a reduction in bond length induced by compressive strain [3,56,57]. This implies that the overall average unit cell volume would be reduced from the straight-type membranes, to the zigzag-type and even more to the spiral-type sample. Literature reports that macrocrystalline 8YSZ pellets can accommodate mechanical stress by a phase change lowering the symmetry [45]. Hence, we tentatively ascribe the larger average unit cell volume in the straight nanomorphology to local monoclinic distortions amid the predominant cubic phase of the 8YSZ free-standing thin films. A reduced elastic modulus implies that less force is required to distort a material, so that less free energy can be gained from a phase change to the monoclinic phase. This may explain why the indications for the monoclinic phase are smaller in the zigzag and more so in the straight nanomorphologies.

Now we turn to investigate the implication of strain and phase change on oxygen ionic transport for the 8YSZ membranes with the straight, zigzag, spiral-shaped nanomorphologies through electrochemical impedance spectroscopy. The cross-plane oxygen ion conductivity was measured, in the direction of the ion transport in micro energy converting devices on a chip, see Fig. 4a. Fig. 4b and c are representative examples of the complex impedance plane plots (Nyquist plots) of zigzag structured 8YSZ samples displayed for the low and high-temperature impedances, at  $300 \text{ }^\circ\text{C}$  and  $510 \text{ }^\circ\text{C}$ , respectively. The

impedance plot at  $300 \text{ }^\circ\text{C}$  consists of a high-frequency shoulder and a much larger low-frequency feature from which only the beginning of the plot is shown and considered in the fit. Based on a comparison of frequencies, the contributions of the resistance associated with wiring and current collection ( $R_s$ ), the electrolyte ( $R_{ysz}$ , including the grain and grain boundary part), and the electrode ( $R_e$ ) can be assigned; the equivalent circuit model of a resistance  $R$  in parallel with a constant phase element  $Q$  is shown in the inset of Fig. 4b. At high temperature, as shown in Fig. 4c, the high-frequency feature cannot be measured for the characteristic frequency over the limit of the impedance analyzer ( $1 \text{ MHz}$ ). The resistance deduced from the offset contains the contribution of the wiring and current collection, which is not negligible where the total resistance is very small. More details and literature reporting similar analysis can be found in methods part and Ref. [58,59]. Based on the equivalent circuit model, we plot the conductivity in an Arrhenius diagram and compare to literature, Fig. 4d. The conductivity for all three nanomorphology types is in agreement with the conductivity of a previous study of 8YSZ free-standing membranes [58] and in line with the grain interior conductivity reported for 8YSZ polycrystalline pellets [60]. Differences in the conductivity of the 8YSZ membranes become most apparent in the low-temperature range ( $200 \text{ }^\circ\text{C}$  to  $265 \text{ }^\circ\text{C}$ ), where changes of the ionic conductivity from straight to the spiral, by a factor of 2 are measurable. We observe that the spiral-structured membrane exhibits the largest cross-plane conductivity while with the straight nanomorphology shows the lowest. Comparable activation energies of around  $1.1 \text{ eV}$  are determined by fitting the linearized Arrhenius equation for all membrane structures, in agreement with the literature [58,60]. Overall, although the slight changes observed, we can conclude that the ionic conductivity is not significantly affected by the nanomorphology modifications. Therefore, we can substantially improve the mechanical stability of the membranes still maintaining the good conduction properties of the films.

### 3. Conclusions

In conclusion, we designed and fabricated Ytria-stabilized zirconia thin films with straight columnar, zigzag and spiral-type nanomorphologies by oblique angle pulsed laser deposition. The variation of morphology from the typically straight columnar to the spiral-type results in nearly a 44% reduction of the elastic modulus. The study on the survival rate during the microfabrication of membranes confirmed the hands-on increased mechanical stability; viz. reduced brittleness for the

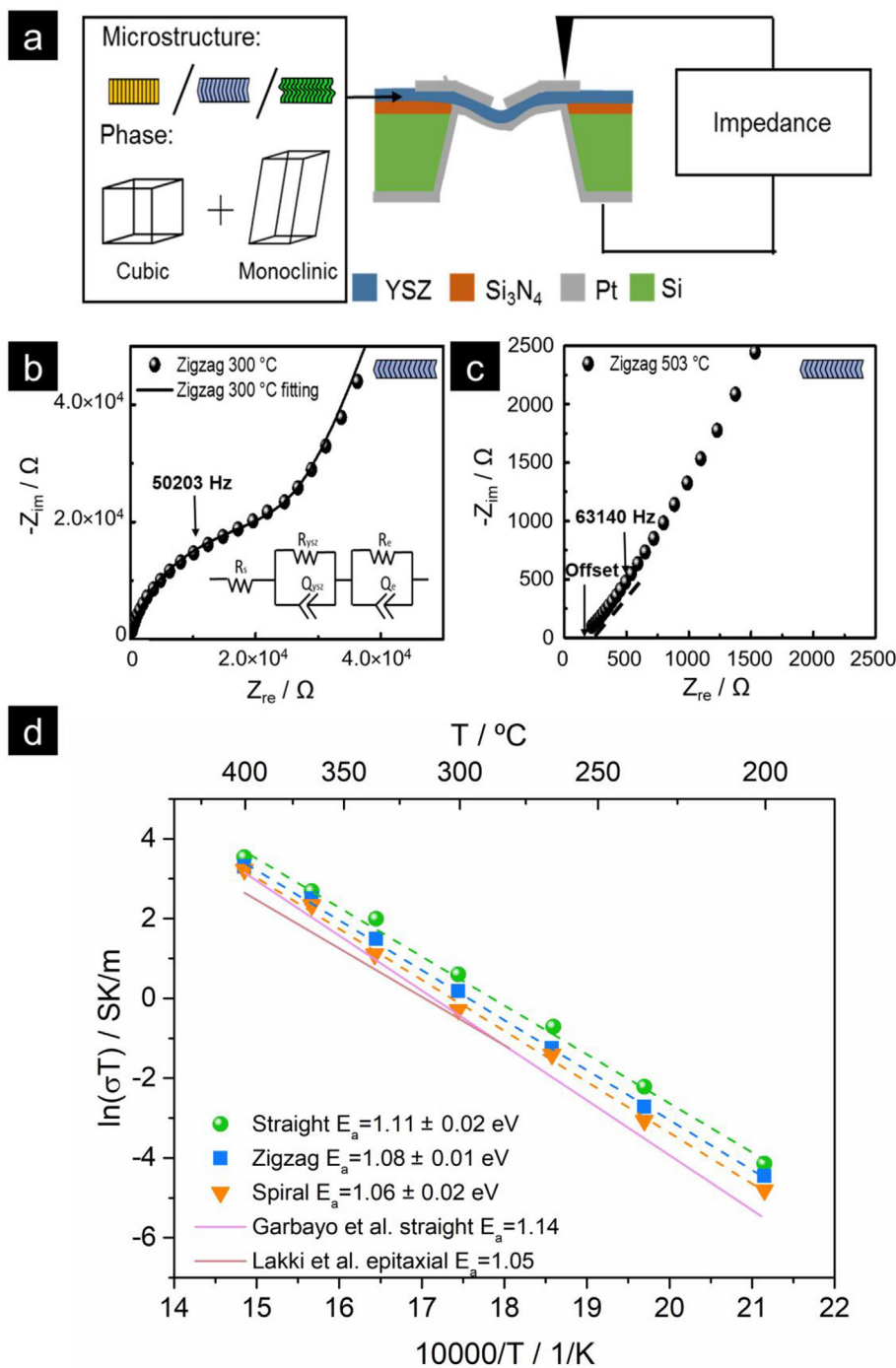


**Fig. 4.** The result of the cross-plane electrical characterization via impedance spectroscopy: (a) Scheme of the cross-plane ionic conduction measurement of free-standing membranes with different nanomorphologies through impedance spectroscopy. (b) High frequency part of the complex impedance plane plot of a zigzag thin film measured at 300 °C, the inset shows the equivalent circuit used to fit the experimental data. (c) High frequency part of the complex impedance plane plot of a zigzag thin film measured at 503 °C. The contribution of the YSZ electrolyte, wiring and current collectors corresponds to the offset. (d) Arrhenius type diagrams of cross-plane total ionic conductivity for the straight, zigzag and spiral-shaped free-standing membranes, as well as the reference from Garbayo et al. (free-standing membrane, straight columnar morphology), Lakki et al. (bulk conductivity of sintered pellet). The activation energies of all the samples are also listed.

ceramic membranes. Raman spectroscopy revealed further that the films exhibit cubic phase with monoclinic distortions as deduced from a redshift in the Raman modes. Partial phase transition from cubic to monoclinic was induced by lowering the symmetry through the accommodation of lattice distortions. Finally, impedance spectroscopy demonstrated that the improved mechanical stability has no negative effect on the ionic transport properties. These results are of strong interest for a wide range of free-standing membrane-based nanomechanical applications, not limited to energy applications [61]. Especially, it opens a new promising prospect of improving the fabrication yield for free-standing oxide membranes with high mechanical stability for energy conversion devices like micro solid oxide fuel cells.

## 4. Experimental

### 4.1. Sample microfabrication

To microfabricate the free-standing membranes of YSZ, substrates of 380 μm thick, 4-inch (100) silicon wafers with double side 200 nm thick low-stress Si<sub>3</sub>N<sub>4</sub> layers coated by low pressure-chemical vapor deposition were made (LP-CVD, Ceramics Laboratory, EPFL). The first step is to define the membrane areas through photolithography (photoresist ma-N1420, micro resist technology GmbH, Germany) and reactive ion etching (RIE, Oxford Instruments RIE 80 +); after that wet etching was applied to remove the Si substrate to get the free-standing Si<sub>3</sub>N<sub>4</sub> thin film template, which is, immersing the wafer in a KOH solution (30

mass %) at 90 °C for 7–8 h. Then the YSZ thin films were deposited by pulsed laser deposition (PLD) on such substrates. A rod target of 8YSZ was ablated with a 248 nm KrF excimer laser (Lambda physics) with a pulse length of 25 ns and a repetition rate of 5 Hz. The spot size on the target was 1.4 mm<sup>2</sup> and a fluence of 3 J/cm<sup>2</sup> was used. The ablation was carried out in a UHV chamber at an oxygen partial pressure of 10<sup>-2</sup> mbar, and the sample was heated to 600 °C. The target to substrate distance was set to 5 cm. For an angle of incidence of the incoming particle flux of 0°, the substrate faced the target and for 60°, the sample holder was tilted. The sample holder can be rotated around the substrate normal which was employed to fabricate the zigzag and the spiral-shaped structures.

The Si<sub>3</sub>N<sub>4</sub> layers underneath the 8YSZ films were removed by a second RIE step from the backside after the Pt microelectrodes on the front side (cathode) were deposited through a shadow mask to release the YSZ free-standing membranes. Finally, the Pt electrode was deposited on the backside (anode) as well. A more detailed fabrication flow to obtain membranes through wet etching and microfabrication can be found in Supplementary Information S4. The top and bottom electrodes are not symmetric, however, the error associated to the calculation of ionic conductivity is negligible as the electrolyte is very thin (in nm range) compared with the electrode size (in μm range). The preferential conduction lines will be straight across the YSZ film and the small thickness of electrolyte make the lateral contribution to the conductivity calculation negligible.

#### 4.2. X-ray diffraction and scanning electron microscopy

The samples were characterized by x-ray diffraction in a Siemens D500 diffractometer with CuK<sub>α</sub> radiation. Scanning electron microscopy (SEM) was employed to characterize the nanomorphology in cross-sectional images with a Zeiss Supra VP55. SEM samples were coated with 10 nm Pt by sputtering to avoid charging of the electrically insulating thin films. Images were recorded with a working distance of 5 mm and an acceleration voltage of 10 kV using an in-lens detector. To perform the nanoindentation test, 8YSZ was deposited the same way (TS = 4 cm) on an Al<sub>2</sub>O<sub>3</sub> substrate (CrysTec GmbH).

#### 4.3. Nanoindentation characterization

Nanoindentation measurements using a Berkovich tip were performed on YSZ films deposited on Al<sub>2</sub>O<sub>3</sub> substrates. 30 experiments were performed on each sample using a Hysitron Ubi (Hysitron Inc., USA) in load control up to 3 mN of maximum force, with 10s loading, hold and unloading time. This protocol allowed to probe depths smaller than 10% of the film thickness, which eliminates significant substrate effects. After the experiments were done, curves with unusual shapes indicating unsuccessful experiments were removed from the dataset. The tip area function was calibrated by indentation in a fused silica reference sample to different depths and indentation modulus, as well as hardness, were measured following the method presented by Oliver and Pharr [62].

#### 4.4. Vibrational Raman spectroscopy

Micro-Raman spectroscopy was carried out on a WITec Alpha300 (Germany) equipped with a 532 nm wavelength laser with a power of 5 mW, a 300 g/mm grating, and lateral resolution of 515 nm. For each sample, 5 Raman measurements were performed at the center of membranes (different positions in an area of 20 μm), and the mean value of Raman peak centers were calculated after fitting etch spectra by Gaussian function in Origin 9.1.

#### 4.5. Microelectrode processing and electrical characterization

Pt microelectrodes were 100 nm thick and were deposited by

electron beam evaporation (physical vapor deposition, Evaporation Plassys II). For the electrical characterization, a custom-made microprobe station was used (Electrochemical Materials Group, ETH Zürich, Switzerland and Everbeing Taiwan), in which electrically shielded micro-manipulators were equipped for electrochemical impedance spectroscopy measurement. The temperature can be controlled up to 550 °C by a hotplate with a thermocouple. Besides that, in-situ microscopy was integrated for observing the sample. The AC electrochemical impedance spectroscopy measurement was processed by instrument Reference 600 (Gamry Instruments, USA), and all measurements were performed between the same pin of the microelectrode design shown in Fig. 1b, and the bottom electrode in a cross-plane arrangement. Z-plot was used to fit the equivalent circuit.

As in the reference of Garbayo et al., the impedance spectrum contains the contribution from wiring and current collecting resistance ( $R_s$ ), YSZ thin film electrolyte ( $R_{YSZ}$  and  $Q_{YSZ}$ ) at high frequency (in this case the part of bulk and grain boundary cannot be distinguished), and the contribution of the electrode ( $R_e$  and  $Q_e$ ) at low frequency [58]. The equivalent circuit is shown in the inset of Fig. 4b. At low temperature (< 400 °C), after fitting, the  $R_s$  is very small and negligible compared to  $R_{YSZ}$ , so the first semicircle is the contribution of the electrolyte. At high temperature (> 400 °C), as in Fig. 4c, the high-frequency feature cannot be measured, because its characteristic frequency is above the limit of the impedance analyzer (1 MHz). In this case only the sum of  $R_s$  and  $R_{YSZ}$  can be determined in terms of the offset as shown in Fig. 4c. Due to the much lower electrolyte resistance,  $R_s$  is unneglectable at this temperature. Therefore, in the experiment, only the results measured in the temperature range 200 °C–400 °C were selected for analysis.

#### Acknowledgments

Andreas Nening, from Electrochemical Materials ETH Zürich, is thanked for helpful discussion of the electrochemical impedance spectroscopy data. We also thank the staff of FIRST Center for Micro- and Nanoscience, ETH Zürich, for providing and maintaining the cleanroom facilities used for the microfabrication described herein. Finally, this work was supported by the Swiss National Science Foundation under the project numbers 144988, 147190, 138914, and ERC SNSF Starting Grant, project number BSSGIO\_155986/1.

#### Appendix A. Supplementary data

Supplementary data to this article can be found online at <https://doi.org/10.1016/j.nanoen.2019.03.017>.

#### References

- [1] A. Evans, A. Bieberle-Hütter, J.L.M. Rupp, L.J. Gauckler, *J. Power Sources* 194 (1) (2009) 119–129.
- [2] I. Garbayo, D. Pla, A. Morata, L. Fonseca, N. Sabaté, A. Tarancón, *Energy Environ. Sci.* 7 (11) (2014) 3617–3629.
- [3] Y. Shi, A.H. Bork, S. Schweiger, J.L.M. Rupp, *Nat. Mater.* 14 (7) (2015) 721–727.
- [4] J.F.M. Oudenhoven, L. Baggetto, P.H.L. Notten, *Adv. Energy Mater.* 1 (1) (2011) 10–33.
- [5] S. Afyon, F. Krumeich, J.L.M. Rupp, *J. Mater. Chem.* 3 (2015) 18636–18648.
- [6] J. van den Broek, S. Afyon, J.L.M. Rupp, *Adv. Energy Mater.* 6 (19) (2016) 1600736.
- [7] M. Rawlence, I. Garbayo, S. Bücheler, J.L.M. Rupp, *Nanoscale* 8 (2016) 14746–14753.
- [8] R. Pfenninger, M. Struzik, I. Garbayo, S. Afyon, J.L.M. Rupp, *Adv. Funct. Mater.* 28 (21) (2018) 1800879.
- [9] I. Garbayo, M. Struzik, W.J. Bowman, R. Pfenninger, E. Stilp, J.L.M. Rupp, *Adv. Energy Mater.* (2017) in press.
- [10] R. Waser, R. Dittmann, G. Staikov, K. Szot, *Adv. Mater.* 21 (25–26) (2009) 2632–2663.
- [11] F. Messerschmitt, M. Kubicek, S. Schweiger, J.L.M. Rupp, *Adv. Funct. Mater.* 24 (47) (2014) 7448–7460.
- [12] F. Messerschmitt, M. Kubicek, J.L.M. Rupp, *Adv. Funct. Mater.* 25 (2015) 5117–5125.
- [13] M. Kubicek, R. Schmitt, F. Messerschmitt, J.L.M. Rupp, *ACS Nano* 9 (11) (2015) 10737–10748.

- [14] S. Schweiger, R. Pfenninger, W.J. Bowman, U. Aschauer, J.L.M. Rupp, *Adv. Mater.* 29 (15) (2016) 1605049.
- [15] R. Schmitt, J. Spring, R. Korobko, J.L.M. Rupp, *ACS Nano* 11 (9) (2017) 8881–8891.
- [16] J.L.M. Rupp, B. Scherrer, N. Schäuble, L.J. Gauckler, *Adv. Funct. Mater.* 20 (17) (2010) 2807–2814.
- [17] S. Omar, E.D. Wachsman, J.C. Nino, *Solid State Ionics* 178 (2008) 1890–1897.
- [18] S. Omar, E.D. Wachsman, J.L. Jones, J.C. Nino, *J. Am. Ceram. Soc.* 92 (11) (2009) 2674–2681.
- [19] J.L.M. Rupp, E. Fabbri, D. Marrocchelli, J.-W. Han, D. Chen, E. Traversa, H.L. Tuller, B. Yildiz, *Adv. Funct. Mater.* 24 (11) (2014) 1562–1574.
- [20] M.J.D. Rushton, A. Chronos, S.J. Skinner, J.A. Kilner, R.W. Grimes, *Solid State Ionics* 230 (2013) 37–42.
- [21] J.L.M. Rupp, *Solid State Ionics* 207 (2012) 1–13.
- [22] N. Schichtel, C. Korte, D. Hesse, N. Zakharov, B. Butz, D. Gerthsen, J. Janek, *Phys. Chem. Chem. Phys.* 12 (43) (2010) 14596–14608.
- [23] S. Schweiger, M.M. Kubicek, F. Messerschmitt, C. Murer, J.L.M. Rupp, *ACS Nano* 8 (5) (2014) 5032–5048.
- [24] D. Pergolesi, V. Roddatis, E. Fabbri, C.W. Schneider, T. Lippert, E. Traversa, J.A. Kilner, *Sci. Technol. Adv. Mater.* 16 (1) (2015) 15001.
- [25] B. Yildiz, *MRS Bull.* 39 (2) (2014) 147–156.
- [26] M. Kubicek, Z. Cai, W. Ma, B. Yildiz, H. Hutter, J. Fleig, *ACS Nano* 7 (4) (2013) 3276–3286.
- [27] S. Sanna, V. Esposito, J.W. Andreasen, J. Hjelm, W. Zhang, T. Kasama, S.B. Simonsen, M. Christensen, S. Linderth, N. Pryds, *Nat. Mater.* 14 (2015) 1–5.
- [28] C.-C. Chao, C.-M. Hsu, Y. Cui, F.B. Prinz, *ACS Nano* 5 (7) (2011) 5692–5696.
- [29] K. Kerman, B. Lai, S. Ramanathan, *J. Power Sources* 196 (5) (2011) 2608–2614.
- [30] J.H. Shim, C.-C. Chao, H. Huang, F.B. Prinz, *Chem. Mater.* 19 (15) (2007) 3850–3854.
- [31] M. Tsuchiya, B.-K. Lai, S. Ramanathan, *Nat. Nanotechnol.* 6 (5) (2011) 282–286.
- [32] A. Evans, J. Martynczuk, D. Stender, C.W. Schneider, T. Lippert, M. Prestat, *Adv. Energy Mater.* 5 (1) (2015) 1–9.
- [33] M.V.F. Schlupp, M. Prestat, J. Martynczuk, J.L.M. Rupp, A. Bieberle-Hütter, L.J. Gauckler, *J. Power Sources* 202 (2012) 47–55.
- [34] B. Scherrer, S. Heiroth, R. Hafner, J. Martynczuk, A. Bieberle-Hütter, J.L.M. Rupp, L.J. Gauckler, *Adv. Funct. Mater.* 21 (20) (2011) 3967–3975.
- [35] U.P. Muecke, A.B. Daniel Beckel, A. Bieberle-hu, S. Graf, A. Infortuna, P. Müller, J.L.M. Rupp, J. Schneider, L. Gauckler, *J. Adv. Funct. Mater.* 18 (2008) 3158–3168.
- [36] H. Huang, M. Nakamura, P. Su, R. Fasching, Y. Saito, F.B. Prinz, *J. Electrochem. Soc.* 154 (1) (2007) 20–24.
- [37] S. Kang, P.C. Su, Y.I. Park, Y. Saito, F.B. Prinz, *J. Electrochem. Soc.* 153 (3) (2006) A554–A559.
- [38] S. Heiroth, R. Ghisleni, T. Lippert, J. Michler, A. Wokaun, *Acta Mater.* 59 (6) (2011) 2330–2340.
- [39] D. Stender, N. Schäuble, A. Weidenkaff, A. Montagne, R. Ghisleni, J. Michler, C.W. Schneider, A. Wokaun, T. Lippert, *Apl. Mater.* 3 (1) (2015) 0610411–061047.
- [40] M.M. Hawkeye, M.T. Taschuk, M.J. Brett, *Glancing Angle Deposition of Thin Films: Engineering the Nanoscale* Chapter 2 John Wiley & Sons, Ltd, 2014.
- [41] A. Barranco, A. Borrás, A.R. González-Elipé, A. Palmero, *Prog. Mater. Sci.* 76 (2016) 59–153.
- [42] J. Lintymer, N. Martin, J. Chappe, P. Delobelle, J. Takadoum, *Surf. Coating Technol.* 200 (2005) 269–272.
- [43] E. Jiménez-piqué, L. González-garcía, V.J. Rico, A.R. González-elipe, *Thin Solid Films* 550 (2014) 444–449.
- [44] J. Lintymer, N. Martin, J.M. Chappé, J. Takadoum, P. Delobelle, *Thin Solid Films* 503 (1–2) (2006) 177–189.
- [45] S. Hart, J. Wallis, I. Sigalas, *Phys. B+C* 139–140 (C) (1986) 183–186.
- [46] J. Sung, P.S. Nicholson, *J. Am. Ceram. Soc.* 71 (9) (1988) 788–795.
- [47] D. Stender, *Controlling Strain and Micro-structure of Yttria Stabilized Zirconia Thin Films Grown by Pulsed Laser Deposition*, PhD Thesis ETH Zürich, 2013.
- [48] S. Heiroth, R. Frison, J.L.M. Rupp, T. Lippert, E.J. Barthazy, E. Müller, M. Döbeli, K. Conder, A. Wokaun, L.J. Gauckler, *Solid State Ionics* 191 (1) (2011) 12–23.
- [49] H.B. Wang, C.R. Xia, G.Y. Meng, D.K. Peng, *Mater. Lett.* 44 (2000) 23–28.
- [50] J.L.M. Rupp, A. Infortuna, L. Gauckler, *J. Acta Mater.* 54 (7) (2006) 1721–1730.
- [51] Robert P. Ingel, David Lewis III, *J. Am. Ceram. Soc.* 71 (4) (1988) 265–271.
- [52] S. Heiroth, *Pulsed Laser Deposition of Functional Electroceramic Thin Films for Micro Solid Oxide Fuel Cell Applications*, ETH Zürich, 2010 Doctoral thesis.
- [53] A. Feinberg, C.H. Perry, *J. Phys. Chem. Solids* 42 (1981) 513–518.
- [54] F. Zhang, C. Chen, J.C. Hanson, R.D. Robinson, I.P. Herman, S. Chan, *J. Am. Ceram. Soc.* 89 (3) (2006) 1028–1036.
- [55] I. Kosacki, V. Petrovsky, H.U. Anderson, P. Colomban, *J. Am. Ceram. Soc.* 85 (11) (2002) 2646–2650.
- [56] Z.H. Ni, T. Yu, Y.H. Lu, Y.Y. Wang, Y.P. Feng, Z.X. Shen, *ACS Nano* 2 (11) (2008) 2301–2305.
- [57] H. Sakata, G. Dresselhaus, M.S. Dresselhaus, M. Endo, *J. Appl. Phys.* 63 (1988) 2769–2772.
- [58] I. Garbayo, A. Tarancón, J. Santiso, F. Peiró, E. Alarcón-LLadó, A. Cavallaro, I. Gràcia, C. Cané, N. Sabaté, *Solid State Ionics* 181 (5–7) (2010) 322–331.
- [59] A.K. Opitz, J. Fleig, *Solid State Ionics* 181 (15–16) (2010) 684–693.
- [60] A. Lakki, R. Herzog, M. Weller, H. Schubert, C. Reetz, O. Görke, M. Kilo, G.J. Borchardt, *Eur. Ceram. Soc.* 20 (2000) 285–296.
- [61] G. Yoshikawa, T. Akiyama, S. Gautsch, P. Vettiger, H. Rohrer, *Nano Lett.* 11 (3) (2011) 1044–1048.
- [62] W.C. Oliver, G.M. Pharr, *J. Mater. Res.* 7 (6) (1992) 1564–1583.
- [63] R. Srinivasan, R.J. De Angelis, G. Ice, B.H. Davis, *J. Mater. Res.* 6 (6) (1991) 1287–1292.



< /au > **Yanuo Shi**. Yanuo Shi received his PhD degree in Materials Science and Engineering at ETH Zürich in Switzerland. Following his PhD he joined ShanghaiTech University as postdoc to pursue his research interest in the development of ionic conductors and electro-chemo-mechanics for solid oxide fuel cell and other energy conversion applications.



< /au > **Aline Fluri**. After studying Physics at ETH Zurich in Switzerland, Aline Fluri studied during her PhD at the Paul Scherrer Institute the thin film growth of solid oxides by Pulsed Laser Deposition, with a focus on strain and the morphology aiming to tune the ion conduction. As a post-doctoral researcher at Kyushu University and the International Institute for Carbon Neutral Energy research, she further investigated whether and how epitaxial strain can influence the surface exchange kinetics in oxide cathode materials for solid oxide fuel cells.



< /au > **Inigo Garbayo**. Inigo holds a M.Sc. in Nanoscience and Nanotechnology and a PhD in Nanoscience from the University of Barcelona (ES), in collaboration with the Institute of Microelectronics of Barcelona IMB-CNM, CSIC (2010, 2013). He has worked as a PostDoctoral researcher at ETH Zürich (CH) (2014–2016) and IREC (ES) (2013–2014 and 2016–2019), as well as a visiting researcher at DTU Energy Conversion (DK) (2012) and SPMS, École Centrale Paris (FR) (2010). Inigo's career has been always related to the development of new materials for energy applications and their transferability to thin films. He has experience in thin film deposition and integration in mainstream silicon technology of functional ceramics for different powering devices, including micro solid oxide fuel cells and solid state micro batteries.



< /au > **J. Jakob Schwiedrzik**. Jakob Schwiedrzik studied Mechanical Engineering at Vienna University of Technology and got his PhD in Biomedical Engineering from University of Berne in 2014 on the topic of bone micromechanics. He joined Empa as a Postdoc the same year working on thin film mechanics and scientific instrument development. In 2018, he started a junior research group on Biomechanics Research based on a SNSF Ambizione grant. His main research interests lie in the identification of nanoscale deformation mechanisms and structure-property relationships in complex nanocomposites using combined experimental and modeling approaches.



< /au > **Johann Michler**. Johann Michler studied Materials Science in Erlangen, Germany. He finished his Ph.D. in 1999 at the L'Ecole Polytechnique Fédérale de Lausanne (EPFL), Switzerland. In 2000 he joined Empa, Swiss Federal Laboratories for Materials Science and Technology in Thun and is currently heading the Laboratory for Mechanics of Materials and Nanostructures. His research interests cover a large spectrum from synthesis of thin films via PVD, ALD and electrochemical methods to development of advanced analytical methods to measure mechanical properties at small length scales under extreme conditions. He authored over 300 peer-reviewed papers and is co-founder of two start-up companies.



< /au > **Daniele Pergolesi.** Daniele Pergolesi received his PhD in 2004 at the University of Genova (Italy). He was Postdoctoral Fellow at the Italian National Institute for Nuclear Physics, the University of Rome Tor Vergata, and the University of Florida (USA). In 2009 he joined the National Institute for Materials Science in Japan. Since 2013 he is scientist at the Paul Scherrer Institut in Switzerland. His research interests focus on thin film deposition and characterization of materials for energy conversion and storage, with special attention to the fields of solid state ionics and solar water splitting.



< /au > **Thomas Lippert.** Thomas Lippert is since 2013 titular professor at the *Laboratory of Inorganic Chemistry* at ETH Zurich, where he got also his habilitation in 2002. He is since 2002 head of the *Thin Films and Interfaces* group in the *Paul Scherrer Institute (PSI)*. Thomas Lippert studied Chemistry at the University of Bayreuth, Germany. He went then as a Postdoctoral Fellow to the NIMC in Tsukuba, Japan. After Japan he moved to Los Alamos National Laboratory, USA, where he also became a Technical Staff Member. In 1999 Thomas Lippert went as Senior Scientist to the PSI, Switzerland. Thomas is since 2017 Editor-in-Chief of Applied Physics A.



< /au > **Jennifer Lilia Marguerite Rupp.** Prof. Jennifer Rupp is the Thomas Lord Associate Professor of Electrochemical Materials at the Department of Materials Science and Engineering, and Associate Professor at the Department of Electrical Engineering and Computer Science at MIT. Her research interests lay in developing materials and devices for green and fair-trade energy storage and designing fast neuromorphic computing and sensing of data. Here, ceramic processing and engineering and the design of structure-charge and mass transport reactions is the key. Ethically she believes that material scientists and engineers can make important contributions defining more operation schemes to profit from renewables and transferring the opportunities to society, economy and politics.